

CHAPTER 1

PROGENITOR SEARCH IN SN 1006

1.1. Introduction

The search for a donor star in SN 1572 has not turned up an obvious candidate. However, we have detected two objects (Tycho-B and Tycho-G) exhibiting some unusual properties, which while interesting, ultimately seem inconsistent with the expectations of any viable donor star scenario. Since donor star scenarios are theoretical in their nature and any actual donor star is likely to not exhibit all features predicted by the model. We have reached an impasse with SN 1572 and more detailed observations will likely not provide a definitive answer if either of these two stars were involved in the progenitor system. An obvious way forward is to scrutinize stars in other Type Ia supernova (henceforth SN Ia) remnants and see if any of those have similar properties to Tycho-B or Tycho-G. The remnant of SN 1006 is the ideal object for this kind of follow-up search.

The lack of a central neutron star, observation of several $0.1 M_{\odot}$ of iron inside the remnant Hamilton et al. (1997) and the the high peak luminosity and basic light curve shape (visible for several years Goldstein & Peng Yoke, 1965) all indicate that SN 1006 was a SN Ia. In addition, the remnant has a secure distance, measured by Winkler et al. (2003), who combined the proper motion and the radial velocity of the expanding shell to measure the distance to 2.2 kpc, making SN 1006 the closest of the ancient SN Ia remnants (consistent SN 1006 being the brightest). The geometric center of the remnant has been determined from both X-ray and radio observations (Winkler et al., 2003). The interior of the remnant has been probed with UV background sources (Winkler et al., 2005). This revealed the aforementioned iron core as well as a silicon rich shell. The remnant has been searched for possible SN Ia donor stars previously, and an unusual O-star has been previously identified as a possible donor star to SN 1006.

This unusual O-Star was identified near the centre of SN 1006 by Schweizer & Middleditch (1980) and is now called Schweizer-Middleditch Star (SM-Star). After successful identifications of neutron stars in both the Vela Remnant and the Crab Remnant this was thought to be the third identification of a stellar remnant in ancient supernovae. Subsequent UV spectroscopic follow-up of the SM-Star by Wu et al. (1983), showed strong Fe II with a profile broadened by a few thousand km s^{-1} . In addition, Wu et al. (1983) identified

redshifted Si II, Si III and Si IV lines. Their conclusion was that these absorption lines stem from the remnant and place the **SM-Star** behind the remnant, making it unrelated to **SN 1006**. Although unrelated, the **SM-Star** is an ideal object to probe the remnant and measure upper limits for interstellar extinction ($E(B-V) = 0.1$ Wu et al., 1993; Winkler et al., 2003).

SN 1006 has several properties which make it an ideal place to undertake a progenitor search. Although the remnant is the oldest among the known **SN Ia** remnants, its age is still young enough that the remnant's center is well determined, and the motion of any donor star small enough that only a small area of stars need to be searched. Furthermore, this elapse of 1005 years is a short length of time relative to the timescales of stellar evolution for donor stars (see Marietta et al., 2000). We still expect a potential donor star to be close to the same state as directly after the supernova explosion. In addition, **SN 1006** has a low interstellar extinction, which makes the determination of stellar parameters much less challenging. These serendipitous conditions for the **SN 1006** remnant led us to launch a photometric and spectroscopic campaign to search for the donor star. Our photometric observations were taken at Siding Spring Observatory with the 2.3m Telescope imager. The spectroscopic observations were undertaken with the high resolution multi-object spectrograph FLAMES attached to the Very Large Telescope (VLT).

In Section 1.2 we outline the observations as well as data reduction of the photometric and spectroscopic data. Section 1.3 is split into four subsections, namely radial velocity, stellar rotation and stellar parameters. We conclude this chapter in Section ?? and discuss the possible implications of our initial find as well as outlining some future work.

1.2. Observations and Data Reduction

Our photometry was obtained from images taken with the imager at the 2.3m Telescope at the Siding Spring Observatory. All data was taken on the night of the 11th of May 2004. We exposed for 1860 s in U-Band, 1490 s in B-Band, 788 s in V-Band and 1860 s in I-Band. For calibration purposes we took images of the PG1633 and PG1047 standard star regions in the same filters. The seeing ranged between 1'' and 2''. The data was reduced in the standard way using PyRAF¹.

For the spectroscopy survey we chose the **VLT** instrument FLAMES, which provides high resolution ($R=25,000$) and a large field of view (25') for 130 targets although with a small spectral coverage of 200 Å. We chose the wavelength region from 5139 Å to 5356 Å which contains the gravity sensitive Mg I b Triplet as well as many iron lines to accurately measure metallicity. As the centre of our spectroscopic survey we chose the mean of the X-ray and radio center ($\alpha = 15^h02^m22^s.1$; $\delta = -42^\circ05'49''$ Winkler et al., 2003). We chose a search radius of 120'' which corresponds to 1250 km s⁻¹ at 2.2 kpc. This generous choice, which is more than four times our maximum expected escape velocity (see Figure ??), was made to accommodate any errors in the choice of the center. Although the models predict the surviving companion to be several hundred L_\odot (Marietta et al., 2000), we chose a limiting magnitude of $V = 17.5$ ($0.5 L_\odot(V)$) at 2.2 kpc including extinction of $E(B-V)=0.1$) to have a comfortable margin of error. An exposure time of 3.8 hours was chosen to obtain spectra with high enough quality to measure rotation and basic stellar parameters (S/N ratio > 20) For completeness and to not waste fibres we chose additional stars down to a magnitude limit of $V = 19$, which are only used in radial velocity measurements. These

¹PyRAF is a product of the Space Telescope Science Institute, which is operated by AURA for NASA.

constraints yielded 26 stars with $V < 17.5$ and 53 stars in the bin between $17.5 < V < 19$ (for a total of 79 stars) for our survey (see Figure 1.2). With fibre buttons not being able to be placed less than $11''$ apart, we had to split our candidates over three different setups. The first two setups were observed five times with 2775 s each. We deliberately chose bright stars for the last setup so that it only had to be observed three times with 2775 s each. As only the central $120''$ were crowded we placed spare fibres on three bright stars ($R \approx 10$; 2MASS J15032744-4204463, 2MASS J15031746-4204165, 2MASS J15033195-4202356) located close to the edge of the $25'$ field of view for calibration purposes. Additional spare fibres were placed on sky positions. These were configured to be placed far from 2MASS sources and were subsequently manually inspected using DSS images to be in star free regions. In addition to our night time calibration, which included simultaneous arc exposures

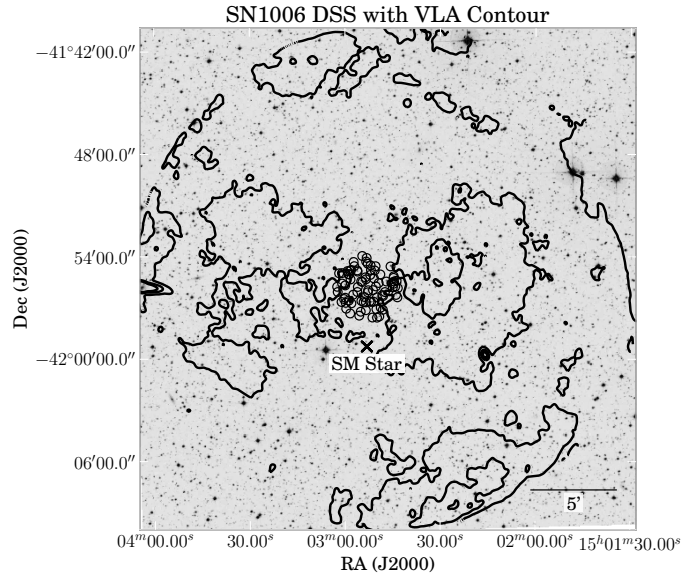


Figure 1.1 Optical DSS image with radio contour overlay (VLA). The black circles in the center show the 79 program stars. Additionally we have marked the ‘spurious’ donor the **SM-Star**.

with four fibres for each observation block, we received standard daytime calibrations. In total, 13 observation blocks with an exposure time of 2775 s each were obtained. Table 1.1 provides the Observing ID, modified julian date, mean seeing, mean airmass, setup name and heliocentric correction for all observations (all data is available under ESO Program ID: 083.D-0805(A)). Due to broken fibres not all stars were observed for the expected length of time. Broken fibres caused SN1006-31 not to be observed at all in this sample (see Figure ??). On the other hand SN1006-31 with $V = 17.87$ is also not considered a candidate.

We first applied a cosmic ray removal tool on the raw 2D frames (van Dokkum, 2001). The data was then reduced with the ESO-CPL pipeline (version 5.2.0), using the GIRAFFE instrument recipes (version 2.8.9). The only change that was made to the default parameters was the usage of the Horne extraction algorithm instead of the "Optimal"-extraction algorithm. This yielded 366 individual spectra of the candidate stars and an additional 39 spectra of the Calibration stars.

For our photometric data reduction we fitted an astrometric solution using astrometry from the 2MASS point source catalogue (Skrutskie et al., 2006) to our frames. We used

Table 1.1 Flames Observations of SN1006 program stars

ObsID	MJD	FWHM	Airmass	Setup name	v_{helio} correction
-	d	"	-	-	km s ⁻¹
360737	54965.1	1.2	1.2	SN1006 1	1.5
360739	54965.1	1.2	1.1	SN1006 1	1.5
360740	54965.1	1.0	1.1	SN1006 1	1.4
360741	54985.0	0.7	1.4	SN1006 1	-7.4
360742	54964.2	1.5	1.1	SN1006 1	1.7
360743	54985.0	0.8	1.2	SN1006 2	-7.5
360745	54985.0	0.9	1.1	SN1006 2	-7.6
360746	54985.1	1.0	1.1	SN1006 2	-7.7
360747	54985.1	1.0	1.1	SN1006 2	-7.7
360748	54985.2	0.9	1.1	SN1006 2	-7.8
360749	54963.1	1.2	1.2	SN1006 3	2.4
360751	54963.1	1.1	1.1	SN1006 3	2.3
360752	54963.2	1.1	1.1	SN1006 3	2.3

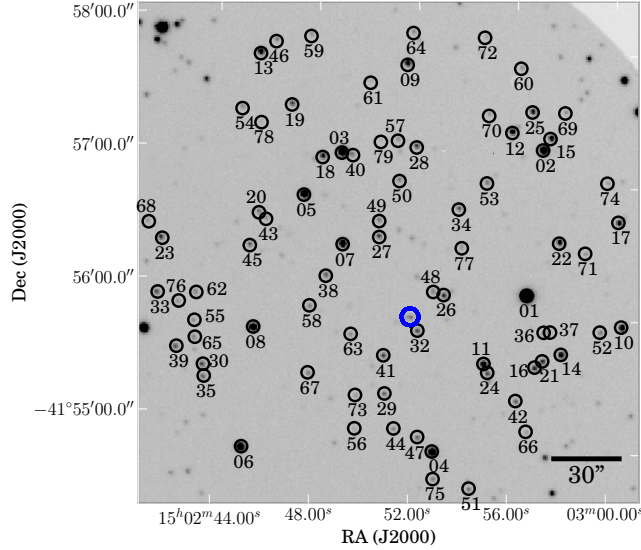


Figure 1.2 V-Band image taken by the 2.3m Telescope. We have marked SN1006-31, which was not observed due to broken fibres, with a blue circle. With the a brightness of $V=17.87$ SN1006-31 is much fainter than $L_{\odot}(V)$ at the distance of 2.2 kpc and would not be considered a donor star candidate.

SExtractor (?) to measure the magnitudes of the objects in the frames and then calibrated our photometry to a standard Bessel Filter system using the Stetson magnitudes ² of our standard fields PG1633 and PG1047 .

The measured magnitudes were supplemented with near infrared magnitudes from the 2MASS point source catalogue (see Table 1.4 and 1.3). Subsequently we checked the photometric measurements, by plotting the obtained $B - V$ colours against the $V - K$ colours (see Figure 1.3).

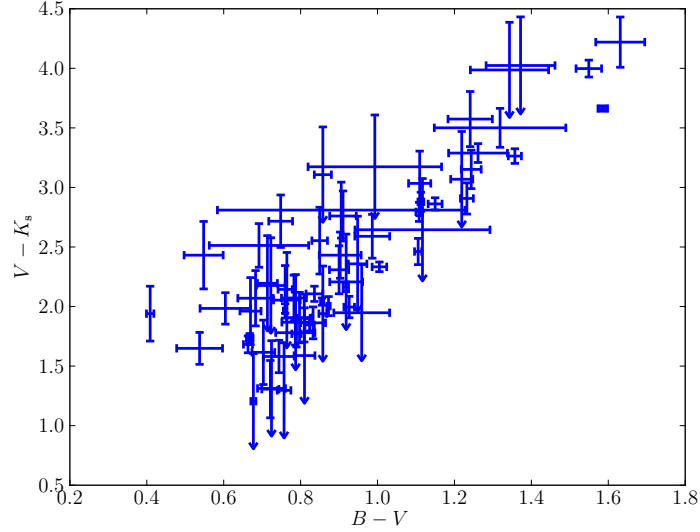


Figure 1.3 Considering the error bars and upper limits for some stars all of the objects lie pretty well on the stellar locus

We have also computed temperatures from photometric colours by using the polynomials given in Casagrande et al. (2010). We assumed an $[\text{Fe}/\text{H}]$ of 0 for all stars, but the choice of $[\text{Fe}/\text{H}]$ only has a minor influence on the temperature calculation (e.g. change of 300K between $[\text{Fe}/\text{H}]=0$ and $[\text{Fe}/\text{H}]=-1$) for the temperature. In addition, the temperature polynomial coefficients incorporating the metallicity are particularly small for the $V - K$ colour. All temperatures are listed in the optical photometry Table 1.3 and infrared photometry Table 1.4.

1.3. Analysis

1.3.1. Radial Velocity

To obtain radial velocities we employ a two step process. We used a solar spectrum from Kurucz et al. (1984) with the standard cross-correlation technique described in Tonry & Davis (1979) and implemented in the IRAF task *fxcor*. The cross-correlation was performed on every single spectra. The results were then heliocentrically corrected, then averaged for each star with a sigma clipping algorithm (see Table 1.5). We note that especially for faint objects we observe a second cross-correlation peak at 0 km s^{-1} and believe that this

²This research used the facilities of the Canadian Astronomy Data Centre operated by the National Research Council of Canada with the support of the Canadian Space Agency

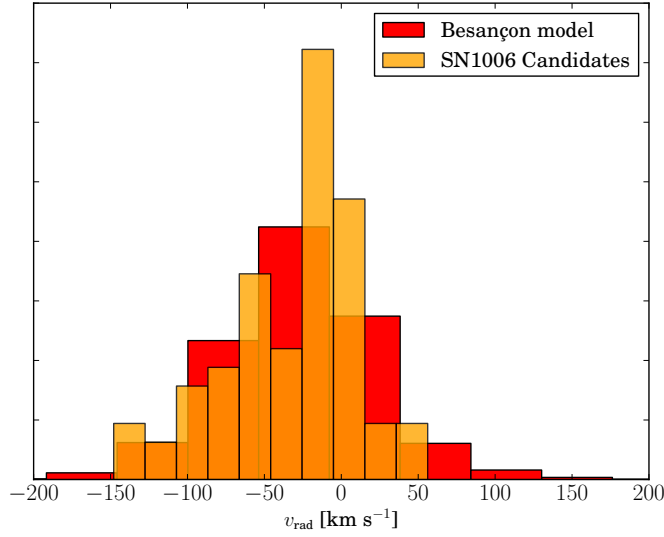


Figure 1.4 Comparison of all candidate stars with the distribution of stars taken from the the Besançon kinematic model. The model input parameters were a search area of 1 square degree around the center of **SN 1006** and a magnitude limit of $10 < V < 17.5$

is reflected light from the moon. We believe that this has a negligible effect on our radial velocity measurement. In Figure 1.4 we have compared our radial velocity measurements with the Besançon kinematic model of the Milky way (Robin et al., 2003). Our selection criteria for creating the Besançon kinematic model was all stars within 1 square degree of **SN 1006** and a magnitude cut of $10 < V < 17.5$. We compared the resulting 10000 stars to our 78 stars in the sample.

1.3.2. Rotational Velocity

Due to the direction looked through the galaxy, there is a large velocity spread in the direction of **SN 1006** (see Figure 1.4). This makes it hard to isolate a donor star based just on kinematic features. A distinguishing feature for a donor star might be rotation (discussed in Chapter ??). The rotational velocities in Chapters ?? & ?? were all measured manually. We selected weak iron lines and stacked them to obtain a line profile, which was compared to synthetically rotationally broadened lines. This was a feasible way for six spectra, it is however not feasible for more than 200 spectra.

Initially we had tried to fit the rotational velocity as an additional parameter in the determination of stellar parameters. For the fainter spectra the optimization algorithm suggested very high rotations. A simple manual inspection revealed that this was not the case.

We realized that in Fourier space it becomes much easier to determine repetitive structures like line profiles. For a description of this method, however we need to review part of the spectral synthesis. The intrinsic spectrum (f_{spectrum}) is created at the photosphere of the star (but already broadened by many factors like thermal broadening and natural broadening). Additionally, the rotation of that star convolves the spectrum with a rotational broadening kernel (g_{rotation}). The light travels to earth and then is convolved again with

the instrumental profile ($h_{\text{instrument}}$) before being recorded on the detector. Let's assume we can create a synthetic spectra matching the intrinsic stellar one which has not been convolved by either rotation or the instrument ($f_{\text{synthetic}}$). A convolution can be described in Fourier space in the following way,

$$f_{\text{observed}} = f_{\text{spectrum}} \otimes \underbrace{g_{\text{rotation}} \otimes h_{\text{instrument}}}_{f_{\text{profile}}}$$

$$F(f_{\text{spectrum}} \otimes g_{\text{rotation}} \otimes h_{\text{instrument}}) = F(f_{\text{spectrum}}) \times F(g_{\text{rotation}}) \times F(h_{\text{instrument}})$$

$$\Rightarrow \frac{F(f_{\text{observed}})}{F(f_{\text{synthetic}})} \approx F(f_{\text{profile}}),$$

where F denotes the Fourier transform. This yields the line profile which we can roughly separate into the instrument profile (using prior knowledge about the resolution of the instrument) and a rotational kernel. This technique is by no means a new idea. It has been described by a selection of authors (e.g. [Gray, 1977](#)). This is the basic method that *fxcor* relies on. *fxcor* however only measures the peak of the profile to estimate the radial velocity. Our collaborator John Laird has used this technique to successfully extract the rotation for some of the stars where the quality of the spectra was adequate (see [Table 1.5](#)).

1.3.3. Stellar Parameters

We obtained detailed stellar parameters for the donor candidates with $V < 17.5$ by employing a grid based technique (three dimensional grid in T_{eff} , $\log g$ and $[\text{Fe}/\text{H}]$). MOOG ([Snedden, 1973](#)) was used to synthesize the spectral grid using the model stellar atmospheres by [Castelli & Kurucz \(2003\)](#). Line wings were taken into account up to 8 Å away from line centre, which seemed to be a reasonable compromise between grid creation time and accuracy. For the atomic lines we merged values from the VALD-2 database ([Kupka et al., 2000](#)) with adjusted values (to reproduce the Arcturus and the Sun) from [Gustafsson et al. \(2008\)](#). In addition, we used the measured molecular lines described in [Kurucz & Bell \(1995\)](#). The final grid extends from 3500 K to 7500 K in T_{eff} with a step size of 250 K, in $\log g$ it ranges from 0 to 5 with a stepsize of 0.5 and in $[\text{Fe}/\text{H}]$ it ranges from -2.5 to 0.5 with a stepsize of 0.5 (with an extra set of points at 0.2).

We used the appropriate sections from the Solar spectrum ([Kurucz et al., 1984](#)) and the Arcturus spectrum ([Hinkle et al., 2000](#)) to calibrate our spectral grid. We measured stellar parameters by first finding the best fitting grid point and then using the minimizer MINUIT to find a minimum by interpolating between the gridpoints (described in Chapter ?? of this thesis; [Barber et al., 1996](#)). For the Sun we obtain stellar parameters of $T_{\text{eff}}=5825$ K, $\log g=4.4$ and $[\text{Fe}/\text{H}]=-0.12$ and for Arcturus we obtain stellar parameters of $T_{\text{eff}}=4336$ K, $\log g=1.9$, $[\text{Fe}/\text{H}]=-0.67$. We acknowledge the error in measurement, but believe our spectral grid to be accurate enough for distinguishing a potential donor candidate against an unrelated star.

To measure our observed spectra we first fitted the continuum with *Legendre polynomials* with a maximum order of 3 and a sigma clipping algorithm discarding the lines. The order that gave the lowest *root mean square* of the fit was used. We then combined the spectra using the previously measured v_{rad} and the computed heliocentric correction. In addition, we broadened the synthetic spectral grid with a rotational kernel for each star where applicable. These spectra were then fit using the previously described algorithm,

Table 1.2 SN 1006 candidates ($V < 17.5$) stellar parameters

Name	T_{eff} K	$\log g$ dex	[Fe/H] dex
01	4285	2.0	-1.0
02	4001	0.8	-1.4
03	5446	4.0	-0.6
04	5347	4.0	-0.6
05	5191	3.7	-0.6
06	5874	4.5	-0.7
07	4884	4.2	-0.8
08	5954	4.2	-0.5
09	4217	3.9	-2.5
10	5662	4.3	-0.8
11	5489	4.1	-0.8
12	5313	4.4	-0.9
13	5114	4.0	-0.7
14	5245	4.3	-0.7
15	5503	4.2	-0.7
16	4448	4.0	-1.8
17	5515	4.4	-1.2
18	5341	4.1	-0.9
19	3846	4.1	-2.4
21	4510	3.1	-1.3
22	6448	4.2	-0.4
23	4429	4.0	-1.8
25	6119	4.9	-0.7
26	5619	4.0	-1.1
27	5336	4.0	-1.3
28	5379	4.3	-1.1

except that we added the $B - V$ photometric temperature as a prior. As the photometric temperature uses the metallicity as an input parameter we recalculated the photometric temperature prior using the metallicity determined by the fit. This procedure was repeated until the gravity estimate converged to less than 0.1 dex. We believe our temperatures to be good to a few hundred K, our surface gravities as well as metallicities have a systematic uncertainty of roughly 0.5 dex.

The stellar parameters can be seen in Figure 1.7 and in tabulated form in Table ???. The final set of stellar parameters shows a usual distribution of many dwarfs and a few giants. None of the stars seem to be unusual in any way.

1.4. Conclusions

In this work we have scrutinized stars to a limit of $0.5 L_{\odot}(V)$ at the distance of the remnant. None of the stars scrutinized in our sample are consistent with the donor star model of [Marietta et al. \(2000\)](#) and [Pakmor et al. \(2008\)](#). For the radial velocity measurements we have shown that the radial velocities of all stars is consistent with a distribution in the direction of [SN 1006](#). Comparing the radial velocity measurements to donor models like (see Figure ?? [Han, 2008](#)) is difficult due to the intrinsically large velocity scatter in the direction of [SN 1006](#). We however note, that we could see the large escape velocity of a main sequence star ($v \approx 170 \text{ km s}^{-1}$). The radial velocity measurements were already ambiguous in [SN 1572](#) and thus we looked for an additional feature namely rotation to discriminate between donor and unrelated stars. None of the stars in our sample have a rotation above $v \sin i = 16 \text{ km s}^{-1}$. We compare these results with the distribution of expected rotational velocities from [Han \(2008\)](#) in Figure 1.5. Again, none of the stars are reconcilable with the donor star models. There is however the caveat of loosing rotation due to expansion (see in ??). This is apriori unlikely (priv. comm. Chris Tout). Finally one could argue that the measurements by [Winkler et al. \(2005\)](#), see Figure 1.6) cast doubt on a precise determination of the center. Their research suggests that the center of the iron core is offset from the geometric center determined by the shocked interstellar medium (ISM). We however argue that this does not mean that the center of mass (where a donor star would reside) is necessarily offcenter. In fact, [Maeda et al. \(2010\)](#) suggest that the iron ejecta is offset from the center of mass, which suggests that the center of the iron core will be different than the center of mass. In summary, this caveat is probably not easily resolved and we will have to hope that our generous choice in radius around the geometric center incorporates any such errors. In addition, other groups are also currently surveying [SN 1006](#) with a larger but photometrically shallower field (priv. comm. Pilar Ruiz-Lapuente) have also not turned up a viable companion. In summary our research shows a consistent result to [SN 1572](#) - no identifiable donor star.

What are the progenitors of [SNe Ia](#)? We have ruled out the standard model of donor stars for [SN 1006](#). A helium white dwarf as a donor star (see Section ??) would not be detectable with our method. It is however unlikely that a helium white dwarf would survive the explosion (priv. comm. Rüdiger Pakmor). The other very real possibility is that [SNe Ia](#) in general or at least [SN 1006](#) do not have donor stars. A double degenerate scenario (DD-scenario) would definitely explain the observational lack of the thought after companion.

A last remnant that can be subjected to such an intensive search is Kepler ([SN 1604](#)). Kepler seems to be different from either [SN 1572](#) and [SN 1006](#) due to detection of interaction with the circumstellar medium (CSM). Observational facts of the Kepler remnant as well as the description of the donor star search will be discussed in the conclusion of this thesis (Chapter ??).

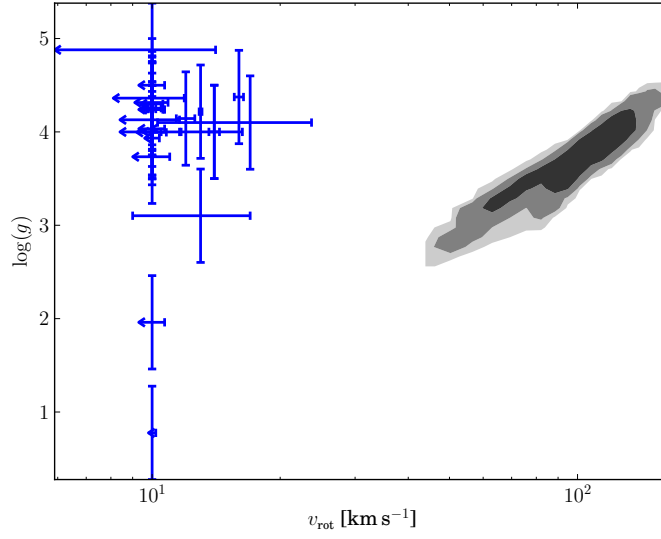


Figure 1.5 Comparison of the evolutionary state and rotational velocity of 55000 binary synthesis SD-Scenario progenitors (gray shades; data from [Han, 2008](#)) with the measured rotation from this work. Due to the resolution of the spectrograph most of these stars only have an upper limit of the rotation speed of $v_{\text{rot}} = 10 \text{ km s}^{-1}$

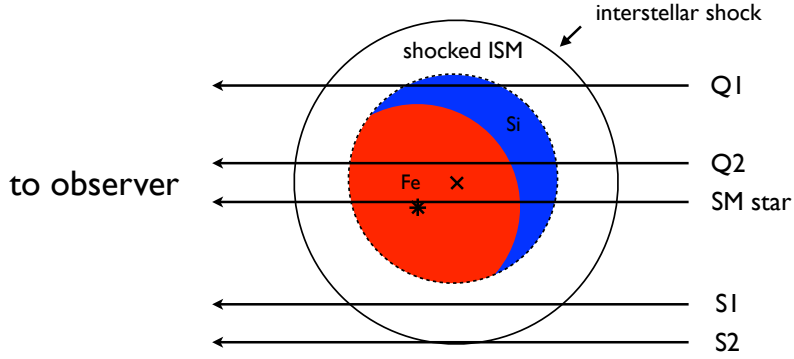


Figure 1.6 Background UV sources probing the remnant. Figure adapted from [Winkler et al. \(2005\)](#)

1.5. Appendix

Table 1.3 [SN 1006](#) optical photometry (Candidates with $V < 17.5$ marked with gray)

Star	RA hh:mm:ss.ss	Dec dd:mm:ss.ss	U mag	σ_U mag	B mag	σ_B mag	V mag	σ_V mag	I mag	σ_I mag
01	15:02:58.27	-41:55:20.9	16.03	0.02	14.76	0.00	13.50	0.08	12.30	0.18
02	15:02:59.95	-41:56:25.2	18.84	0.08	16.96	0.01	15.37	0.01	13.95	0.05
03	15:02:51.80	-41:56:39.9	16.16	0.02	15.86	0.01	15.04	0.01	14.23	0.09
04	15:02:53.35	-41:54:18.0	16.67	0.02	16.33	0.00	15.47	0.00	14.62	0.00
05	15:02:49.97	-41:56:23.9	16.90	0.03	16.41	0.00	15.50	0.01	14.65	0.00
06	15:02:45.68	-41:54:35.2	16.21	0.01	16.17	0.01	15.50	0.00	14.78	0.01
07	15:02:51.19	-41:55:58.5	17.62	0.05	16.91	0.02	15.90	0.01	14.92	0.02

Table 1.3 – continued from previous page

Star	RA	Dec	U	σ_U	B	σ_B	V	σ_V	I	σ_I
	hh:mm:ss.ss	dd:mm:ss.ss	mag	mag	mag	mag	mag	mag	mag	mag
08	15:02:47.00	-41:55:28.3	16.57	0.03	16.53	0.01	15.86	0.01	15.16	0.00
09	15:02:55.07	-41:57:14.4	18.46	0.20	17.73	0.01	16.58	0.01	15.53	0.02
10	15:03:01.87	-41:54:59.2	17.18	0.04	17.06	0.00	16.30	0.00	15.51	0.00
11	15:02:56.05	-41:54:53.5	17.02	0.03	17.12	0.00	16.33	0.05	15.61	0.01
12	15:02:58.83	-41:56:35.5	17.60	0.03	17.22	0.00	16.39	0.02	15.50	0.02
13	15:02:49.22	-41:57:31.1	17.93	0.09	17.41	0.01	16.49	0.00	15.74	0.06
14	15:02:59.24	-41:54:51.6	17.93	0.04	17.44	0.00	16.56	0.00	15.75	0.01
15	15:03:00.33	-41:56:29.8	17.81	0.01	17.42	0.01	16.63	0.01	15.87	0.04
16	15:02:58.09	-41:54:47.9	19.60	0.47	18.37	0.01	17.26	0.00	16.11	0.03
17	15:03:02.49	-41:55:46.7	17.45	0.02	17.40	0.00	16.66	0.04	16.02	0.13
18	15:02:50.99	-41:56:39.4	18.00	0.03	17.61	0.00	16.77	0.03	15.87	0.04
19	15:02:50.12	-41:57:05.5	20.28	0.00	18.75	0.01	17.39	0.01	16.01	0.00
20	15:02:48.03	-41:56:19.4	-	-	19.59	0.03	18.04	0.01	15.97	0.17
21	15:02:58.44	-41:54:50.1	20.60	0.00	18.47	0.01	17.36	0.01	16.30	0.03
22	15:02:59.95	-41:55:41.9	17.26	0.04	17.25	0.00	16.71	0.06	16.18	0.04
23	15:02:43.94	-41:56:15.4	19.62	0.32	18.50	0.01	17.39	0.00	16.24	0.01
24	15:02:56.14	-41:54:49.2	-	-	18.28	0.00	17.59	0.13	16.49	0.11
25	15:02:59.79	-41:56:43.2	17.75	0.01	17.64	0.06	17.03	0.02	16.35	0.03
26	15:02:54.92	-41:55:27.7	18.10	0.10	17.95	0.01	17.23	0.02	16.43	0.00
27	15:02:52.72	-41:55:58.9	18.61	0.08	18.26	0.02	17.47	0.03	16.64	0.05
28	15:02:54.86	-41:56:36.4	18.52	0.13	18.24	0.00	17.43	0.02	16.70	0.02
29	15:02:51.84	-41:54:47.9	-	-	19.23	0.00	18.00	0.02	16.72	0.04
30	15:02:44.71	-41:55:15.4	18.05	0.03	18.24	0.03	17.54	0.02	16.75	0.01
32	15:02:53.61	-41:55:13.7	18.72	0.18	18.42	0.02	17.64	0.03	16.78	0.03
33	15:02:43.38	-41:55:51.5	19.07	0.23	18.56	0.04	17.66	0.04	16.69	0.05
34	15:02:56.13	-41:56:05.1	18.64	0.11	18.52	0.02	17.76	0.01	16.94	0.01
35	15:02:44.66	-41:55:10.0	19.06	0.17	18.74	0.00	17.84	0.02	16.88	0.05
36	15:02:58.70	-41:55:02.9	19.46	0.40	18.65	0.01	17.79	0.01	16.86	0.02
38	15:02:50.29	-41:55:45.6	18.58	0.08	18.48	0.03	17.80	0.03	17.00	0.01
39	15:02:43.76	-41:55:25.6	18.86	0.06	18.44	0.02	17.69	0.01	16.97	0.01
40	15:02:52.23	-41:56:37.9	-	-	-	-	-	-	16.28	0.06
41	15:02:52.06	-41:55:05.2	17.97	0.01	18.02	0.00	17.61	0.01	17.11	0.02
42	15:02:57.08	-41:54:34.3	19.22	0.27	18.78	0.03	17.99	0.01	17.16	0.03
43	15:02:48.27	-41:56:15.9	-	-	20.14	0.04	18.76	0.08	17.25	0.06
44	15:02:51.96	-41:54:31.4	-	-	19.79	0.01	18.54	0.02	17.06	0.01
45	15:02:47.43	-41:56:05.3	18.45	0.11	18.43	0.02	17.71	0.03	17.00	0.05
46	15:02:49.93	-41:57:35.3	20.09	0.17	19.04	0.03	18.05	0.04	17.19	0.20
47	15:02:52.86	-41:54:25.7	18.89	0.24	18.63	0.01	17.96	0.03	17.14	0.03
48	15:02:54.52	-41:55:29.9	-	-	19.29	0.03	18.38	0.01	17.38	0.06
49	15:02:52.83	-41:56:06.1	18.90	0.33	18.84	0.00	18.17	0.01	17.37	0.05
50	15:02:53.93	-41:56:22.6	19.68	0.11	18.99	0.03	18.07	0.03	17.19	0.02
51	15:02:54.58	-41:53:58.4	19.47	0.00	18.90	0.26	17.99	0.19	16.93	0.17
52	15:03:00.97	-41:54:58.6	19.41	0.17	18.89	0.00	18.08	0.03	17.24	0.02

Table 1.3 – continued from previous page

Star	RA	Dec	U	σ_U	B	σ_B	V	σ_V	I	σ_I
	hh:mm:ss.ss	dd:mm:ss.ss	mag	mag	mag	mag	mag	mag	mag	mag
53	15:02:57.45	-41:56:14.7	19.32	0.43	18.90	0.03	18.13	0.01	17.24	0.05
54	15:02:48.09	-41:57:07.7	20.33	0.58	19.40	0.02	18.45	0.01	17.48	0.03
55	15:02:44.67	-41:55:35.9	-	-	19.90	0.01	18.68	0.03	17.36	0.04
56	15:02:50.38	-41:54:34.5	-	-	20.15	0.16	18.83	0.06	17.46	0.08
57	15:02:54.15	-41:56:40.9	19.59	0.57	18.91	0.02	18.26	0.04	17.63	0.07
58	15:02:49.42	-41:55:33.5	18.90	0.09	18.92	0.02	18.21	0.02	17.41	0.02
59	15:02:51.38	-41:57:34.9	19.59	0.37	19.21	0.01	18.54	0.02	17.78	0.02
60	15:02:59.64	-41:57:03.8	20.05	0.18	19.22	0.01	18.48	0.13	18.62	0.43
61	15:02:53.45	-41:57:09.2	-	-	20.49	0.05	19.24	0.02	17.82	0.07
62	15:02:44.94	-41:55:48.3	-	-	19.38	0.02	18.53	0.01	17.54	0.01
63	15:02:50.89	-41:55:17.4	20.19	0.15	19.41	0.00	18.55	0.02	17.62	0.05
64	15:02:55.53	-41:57:28.3	19.45	0.28	18.87	0.02	18.51	0.03	17.87	0.08
65	15:02:44.57	-41:55:28.2	18.79	0.04	18.93	0.03	18.38	0.04	17.63	0.05
66	15:02:57.28	-41:54:19.6	-	-	20.02	0.03	19.09	0.02	18.00	0.03
67	15:02:48.88	-41:55:03.4	19.69	0.38	19.11	0.03	18.37	0.01	17.57	0.01
68	15:02:43.51	-41:56:23.9	20.65	0.00	19.60	0.04	18.75	0.04	17.94	0.01
69	15:03:01.11	-41:56:40.2	20.07	0.00	19.59	0.03	18.59	0.17	17.91	0.09
70	15:02:58.01	-41:56:45.0	20.38	0.57	19.49	0.01	18.73	0.03	18.00	0.06
71	15:03:00.93	-41:55:35.3	-	-	19.95	0.02	18.84	0.02	17.92	0.25
72	15:02:58.39	-41:57:20.6	19.34	0.00	19.90	0.11	18.85	0.11	18.01	0.14
73	15:02:50.64	-41:54:49.5	-	-	20.00	0.04	19.04	0.06	17.92	0.12
74	15:03:02.32	-41:56:05.2	-	-	19.88	0.08	18.76	0.16	18.21	0.02
75	15:02:53.19	-41:54:05.5	19.23	0.11	19.07	0.03	18.34	0.03	17.50	0.03
76	15:02:44.17	-41:55:45.8	19.56	0.09	19.40	0.02	18.70	0.03	17.91	0.08
77	15:02:55.98	-41:55:47.4	19.58	0.20	19.22	0.02	18.56	0.05	17.69	0.02
78	15:02:48.76	-41:56:59.9	-	-	20.87	0.10	19.53	0.01	18.06	0.05
79	15:02:53.45	-41:56:41.7	-	-	21.53	0.06	19.90	0.02	18.04	0.05

Table 1.4 SN 1006 infrared photometry (Candidates with $V < 17.5$ marked in gray)

Star	J	σ_J	H	σ_H	K	σ_K	QFlag	$T_{\text{eff}}(\text{B-V})$	$T_{\text{eff}}(\text{V-K})$
	mag	mag	mag	mag	mag	mag		K	K
01	11.05	0.02	10.32	0.02	10.21	0.02	AAA	4531	4376
02	12.67	0.03	11.87	0.03	11.71	0.02	AAA	3990	4150
03	13.63	0.04	13.26	0.04	13.19	0.05	AAA	5559	5780
04	13.92	0.03	13.56	0.03	13.43	0.03	AAA	5467	5518
05	13.93	0.02	13.50	0.03	13.33	0.04	AAA	5299	5367
06	14.15	0.02	13.82	0.03	13.77	0.04	AAA	6051	5947
07	14.11	0.03	13.68	0.03	13.57	0.04	AAA	5080	5178
08	14.51	0.03	14.32	0.04	14.18	0.07	AAA	6067	6026
09	14.45	0.03	13.85	0.04	13.72	0.05	AAA	4754	4687
10	14.79	0.03	14.37	0.03	14.34	0.06	AAA	5751	5619
11	14.93	0.05	14.69	0.07	14.55	0.09	AAA	5669	5876

Table 1.4 – continued from previous page

Star	J	σ_J	H	σ_H	K	σ_K	QFlag	$T_{\text{eff}}(\text{B-V})$	$T_{\text{eff}}(\text{V-K})$
	mag	mag	mag	mag	mag	mag		K	K
12	14.81	0.04	14.39	0.05	14.28	0.06	AAA	5523	5437
13	14.86	0.04	14.52	0.05	14.49	0.09	AAA	5277	5576
14	15.01	0.04	14.67	0.04	14.56	0.08	AAA	5420	5566
15	15.23	0.04	14.96	0.06	14.86	0.11	AAA	5660	5890
16	15.17	0.07	14.63	0.07	14.47	0.08	AAA	4843	4742
17	15.48	0.06	15.06	0.07	15.08	0.13	AAB	5800	-
18	15.37	0.06	14.99	0.06	14.91	0.13	AAB	5533	-
19	15.00	0.04	14.34	0.05	14.13	0.06	AAA	4356	4393
20	14.92	0.04	14.29	0.05	14.04	0.07	AAA	4044	3978
21	15.41	0.05	14.96	0.06	14.90	0.11	AAB	4849	-
22	15.70	0.07	15.43	0.08	15.06	0.12	AAB	6537	-
23	15.35	0.05	14.76	0.05	14.51	0.08	AAA	4833	4673
24	15.90	0.08	15.22	0.09	15.08	0.13	AAB	5969	-
25	15.56	0.05	15.27	0.06	15.05	0.13	AAB	6278	-
26	16.05	0.09	15.66	0.13	15.92	0.24	ABD	5872	-
27	16.08	0.08	15.59	0.11	15.56	0.21	ABC	5636	-
28	16.08	0.08	15.38	0.09	15.53	0.20	AAC	5600	-
29	15.75	0.06	15.18	0.08	15.09	0.13	AAB	4587	-
30	15.98	0.09	15.72	0.11	15.92	0.27	AAD	5932	-
32	16.17	0.11	15.69	0.12	15.57	0.19	ABC	5680	-
33	16.00	0.08	15.41	0.09	15.23	0.19	AAC	5338	-
34	16.25	0.09	15.54	0.10	15.62	0.20	AAC	5750	-
35	16.08	0.12	15.72	0.12	15.53	0.20	BBC	5346	-
36	16.56	0.13	16.60	0.24	15.85	-	BDU	5461	-
37	-	-	-	-	-	-	nan	-	-
38	16.24	0.08	16.03	0.13	15.73	0.23	ABD	5999	-
39	16.28	0.12	16.16	0.15	16.39	-	BCU	5759	-
40	14.96	0.04	14.28	0.04	14.06	0.05	AAA	-	-
41	16.43	0.11	16.02	0.14	15.67	0.23	ABD	7102	-
42	16.30	0.08	15.98	0.14	16.12	-	ABU	5667	-
43	16.39	0.12	15.49	0.08	14.74	-	BAU	4330	-
44	16.19	0.09	15.39	0.09	15.39	0.16	AAC	4565	-
45	16.59	0.13	15.92	0.12	15.53	-	BBU	5868	-
46	16.52	0.12	15.76	0.12	15.46	0.18	BBC	5125	-
47	16.43	0.11	16.08	0.14	16.00	0.28	ABD	6044	-
48	16.76	0.13	16.04	0.15	15.62	0.21	BBC	5319	-
49	16.72	0.13	16.37	0.18	16.96	-	BCU	6019	-
50	16.59	0.12	15.89	0.14	15.86	-	BBU	5297	-
51	16.72	0.13	16.08	0.15	15.18	0.14	BBB	5331	-
52	16.66	0.12	16.15	0.17	16.49	-	BCU	5598	-
53	16.69	0.13	16.15	0.17	16.08	-	BCU	5736	-
54	16.64	0.13	16.02	-	16.09	-	BUU	5220	-
55	16.50	0.15	15.99	0.14	15.61	-	BBU	4613	-

Table 1.4 – continued from previous page

Star	J	σ_J	H	σ_H	K	σ_K	QFlag	$T_{\text{eff}}(\text{B-V})$	$T_{\text{eff}}(\text{V-K})$
	mag	mag	mag	mag	mag	mag		K	K
56	16.54	0.13	15.72	0.13	15.33	0.15	BBC	4425	-
57	-	-	-	-	-	-	nan	6120	-
58	16.82	0.15	16.78	0.28	16.01	-	BDU	5897	-
59	-	-	-	-	-	-	nan	6017	-
60	-	-	-	-	-	-	nan	5816	-
61	16.50	0.12	15.93	0.13	15.67	0.23	BBD	4570	-
62	17.15	0.23	16.10	0.14	15.98	0.28	DBD	5485	-
63	16.95	0.17	16.15	0.15	15.44	-	CCU	5461	-
64	-	-	-	-	-	-	nan	7316	-
65	17.20	0.20	16.51	0.22	15.95	0.28	CDD	6495	-
66	-	-	-	-	-	-	nan	5274	-
67	16.91	0.18	16.53	0.21	15.65	0.22	CDD	5786	-
68	-	-	-	-	-	-	nan	5495	-
69	16.94	0.14	17.68	-	15.42	-	CUU	5109	-
70	-	-	-	-	-	-	nan	5774	-
71	16.71	0.14	16.42	0.21	15.81	0.27	CCD	4840	-
72	-	-	-	-	-	-	nan	4974	-
73	16.85	0.16	16.11	0.16	17.09	-	CCU	5193	-
74	17.17	0.23	16.00	0.15	16.12	-	DBU	4824	-
75	16.84	0.14	16.73	-	17.03	-	BUU	5862	-
76	-	-	-	-	-	-	nan	5947	-
77	-	-	-	-	-	-	nan	6074	-
78	17.02	0.19	16.11	0.17	15.54	-	CCU	4381	-
79	16.68	0.13	15.87	0.13	15.68	0.21	BBC	3924	-

Table 1.5 SN 1006 candidate kinematics with statistical errors and number of measurements (candidates with $V < 17.5$ marked in gray)

Name	v_{rad}	σ_{rad}	N_{rad}	v_{rot}	σ_{rot}	N_{rot}
	km s ⁻¹	km s ⁻¹		km s ⁻¹	km s ⁻¹	
01	-109.1	0.0	5	< 10	0.7	5
02	56.2	0.4	3	< 10	0.2	3
03	5.9	1.0	3	< 10	0.0	3
04	-14.3	0.0	5	< 10	0.7	5
05	-1.1	0.0	5	< 10	1.0	5
06	-103.9	0.2	5	< 10	0.7	5
07	-76.3	2.1	5	10	0.2	5
08	-0.6	0.2	5	< 10	0.6	5
09	-47.0	0.8	5	< 10	0.4	5
10	-20.2	0.5	5	< 10	0.9	5
11	-5.9	0.3	5	< 10	1.6	5
12	-59.8	0.4	5	16	0.4	5
13	12.3	0.1	5	< 10	1.6	5
14	-17.0	0.4	5	< 10	0.6	5

Table 1.5 – continued from previous page

Name	v_{rad} km s ⁻¹	σ_{rad} km s ⁻¹	N_{rad}	v_{rot} km s ⁻¹	σ_{rot} km s ⁻¹	N_{rot}
15	-72.0	0.2	5	< 10	0.7	5
16	9.4	0.1	5	14	2.3	5
17	-102.1	0.3	5	< 10	1.9	5
18	11.6	0.7	5	12	0.6	5
19	-47.8	0.3	5	17	6.7	4
20	-22.4	0.5	4	-	0.0	2
21	-18.5	0.0	5	13	4.0	4
22	-22.9	0.7	2	13	0.1	2
23	-63.3	1.3	5	14	0.4	4
24	-67.2	0.8	5	10	-	1
25	40.7	0.3	5	< 10	4.1	5
26	-7.0	0.1	5	< 10	0.8	5
27	-52.0	2.1	5	< 10	0.5	5
28	-43.5	0.3	3	< 10	0.5	3
29	-13.3	0.2	4	14	2.3	5
30	-28.2	1.3	3	< 10	0.5	3
32	-104.0	0.3	5	11	3.2	3
33	-120.9	0.2	5	< 10	1.3	4
34	-47.1	0.5	5	< 10	3.0	4
35	-24.6	1.5	5	12	0.9	4
36	-96.7	1.2	3	< 10	-	1
37	-22.7	16.1	4	-	-	-
38	-12.4	2.2	5	< 10	0.8	5
39	22.4	1.3	3	< 10	0.8	2
40	-13.8	8.6	4	-	-	-
41	-4.4	4.3	5	16	1.2	4
42	-64.9	0.3	5	< 10	0.5	3
43	-7.6	1.7	5	-	-	-
44	-28.2	0.2	4	-	-	-
45	-135.4	0.3	5	< 10	3.9	4
46	-13.0	0.3	5	11	0.6	2
47	-0.3	0.1	5	< 10	2.7	4
48	3.6	0.6	3	11	1.9	3
49	-90.4	64.7	3	< 10	1.0	3
50	-82.7	1.5	5	< 10	1.0	5
51	-59.8	0.5	5	14	1.2	2
52	-8.8	1.1	4	-	-	-
53	-63.2	1.3	5	< 10	-	1
54	-51.8	0.0	5	10	1.4	2
55	-24.7	1.5	5	-	-	-
56	-0.0	1.9	4	-	-	-
57	-40.7	2.0	4	-	-	-
58	2.0	0.2	5	< 10	1.5	4

Table 1.5 – continued from previous page

Name	v_{rad} km s ⁻¹	σ_{rad} km s ⁻¹	N_{rad}	v_{rot} km s ⁻¹	σ_{rot} km s ⁻¹	N_{rot}
59	-17.5	0.4	5	< 10	-	1
60	-73.0	2.2	3	< 10	-	1
61	-34.6	24.7	5	-	0.0	5
62	21.2	1.1	3	12	-	1
63	-45.8	42.1	5	14	2.4	2
64	-24.1	0.4	2	< 10	-	1
65	38.3	55.3	3	< 10	-	-
66	-15.4	13.7	2	-	-	-
67	-146.2	1.1	4	< 10	-	1
68	-71.3	0.5	5	10	-	1
69	-47.6	0.4	5	12	0.1	2
70	-23.9	1.0	5	19	1.8	5
71	0.7	0.1	5	14	2.0	5
72	-4.5	5.9	2	-	-	-
73	-8.0	1.0	4	< 10	2.0	2
74	-27.2	23.0	5	-	-	-
75	-147.9	0.4	5	< 10	0.5	3
76	23.3	24.1	5	-	-	-
77	-3.3	3.8	4	-	-	-
78	-7.5	0.3	5	-	-	-
79	-0.6	4.5	4	-	-	-

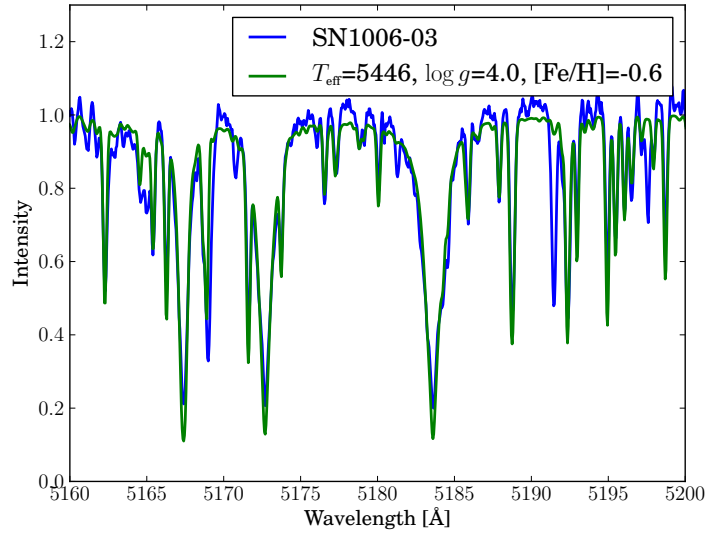
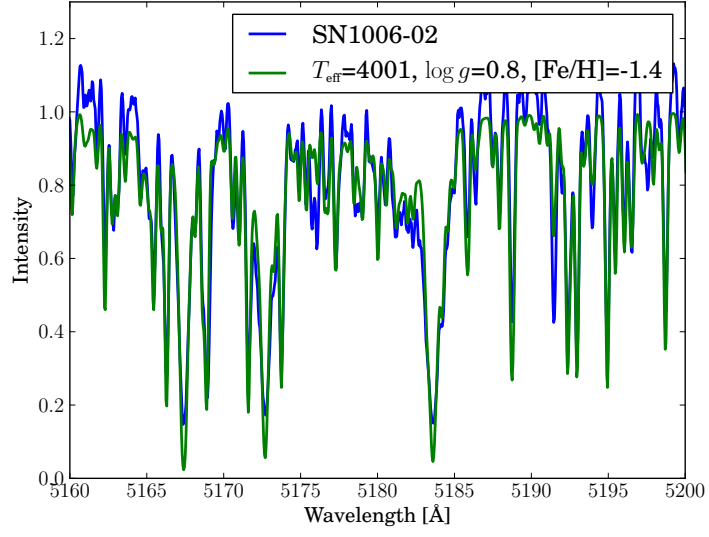
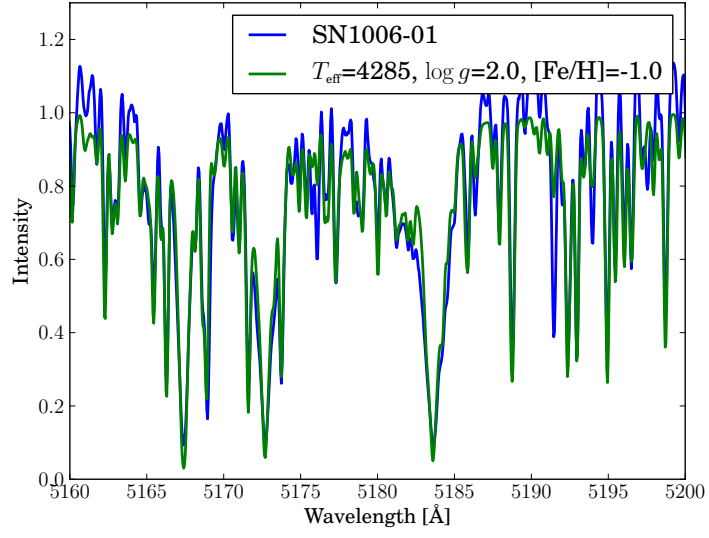


Figure 1.7 Fit of SN1006 candidate spectra

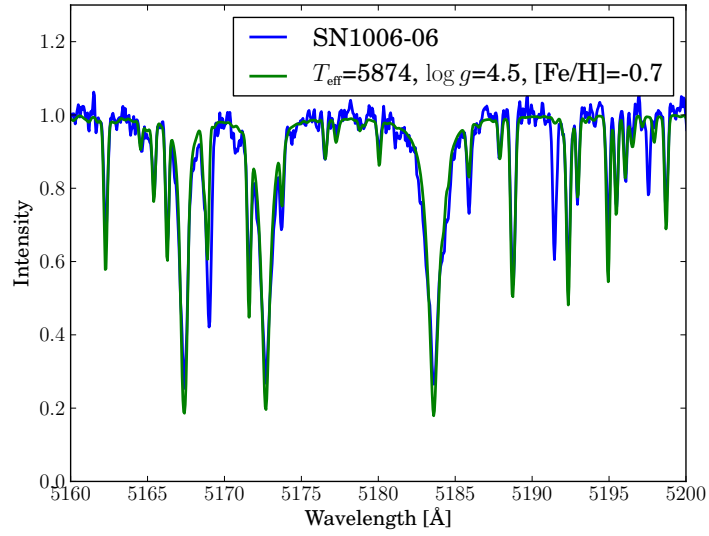
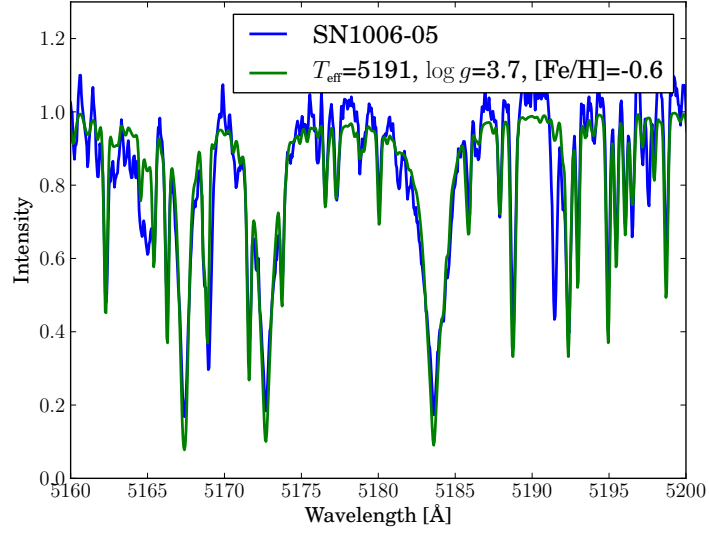
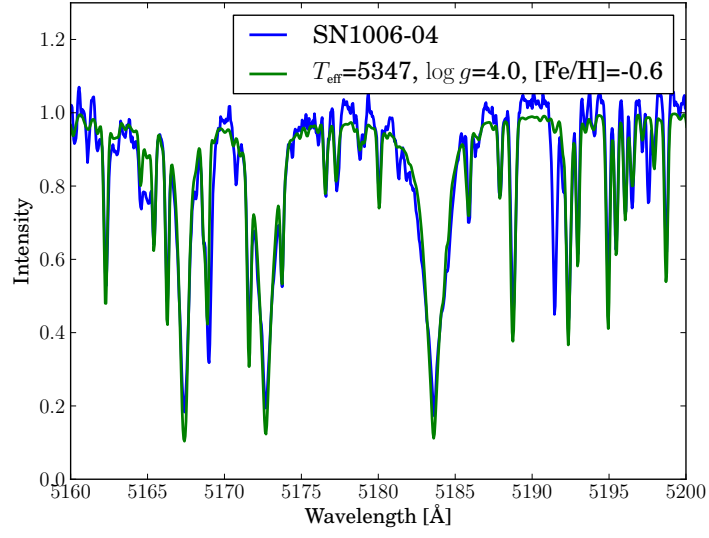


Figure 1.7 Fit of SN1006 candidate spectra

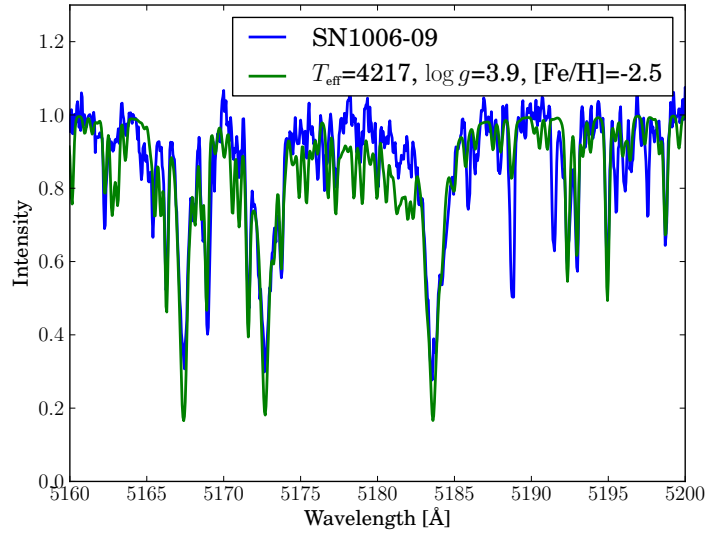
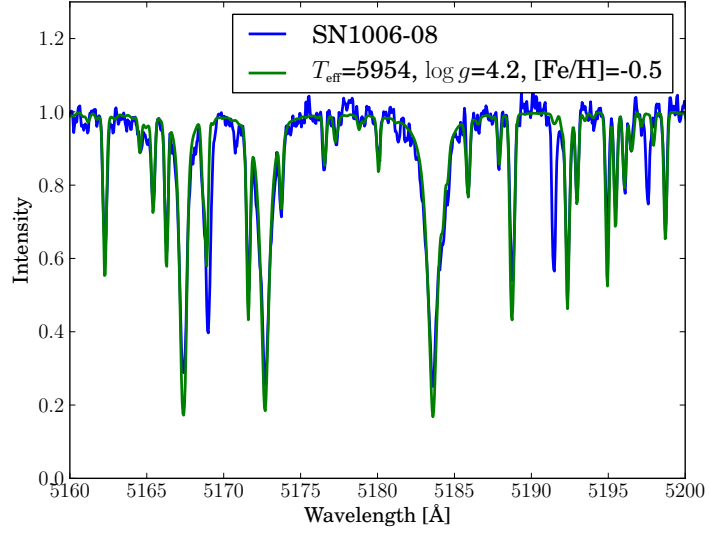
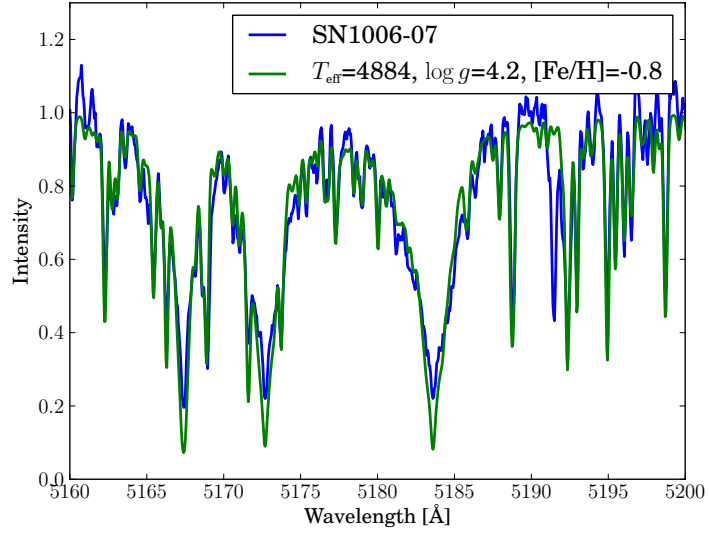


Figure 1.7 Fit of SN1006 candidate spectra

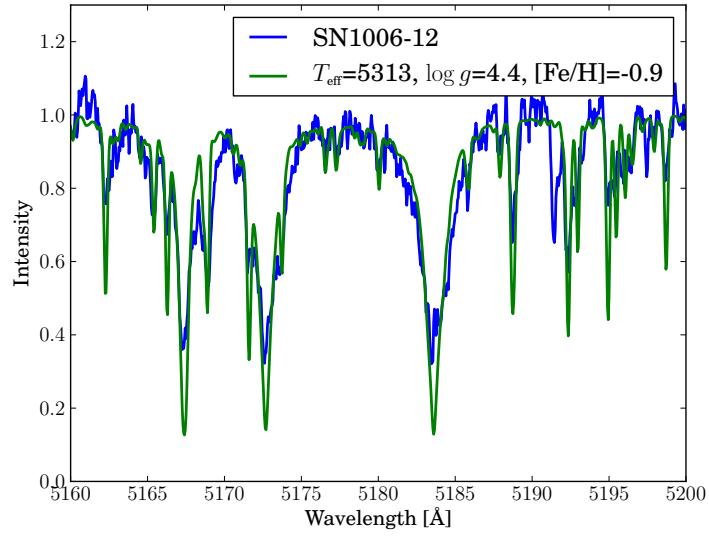
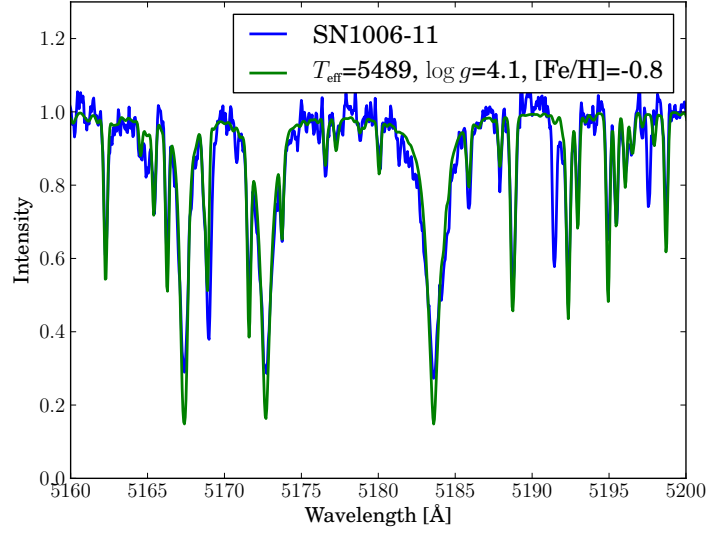
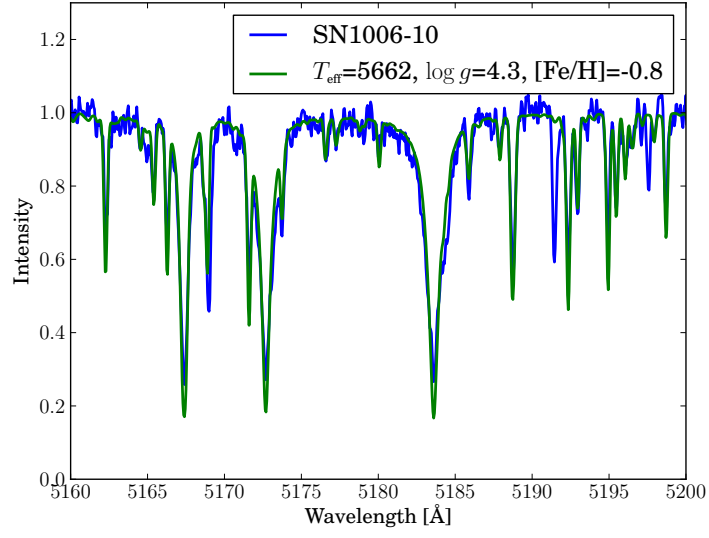


Figure 1.7 Fit of SN1006 candidate spectra

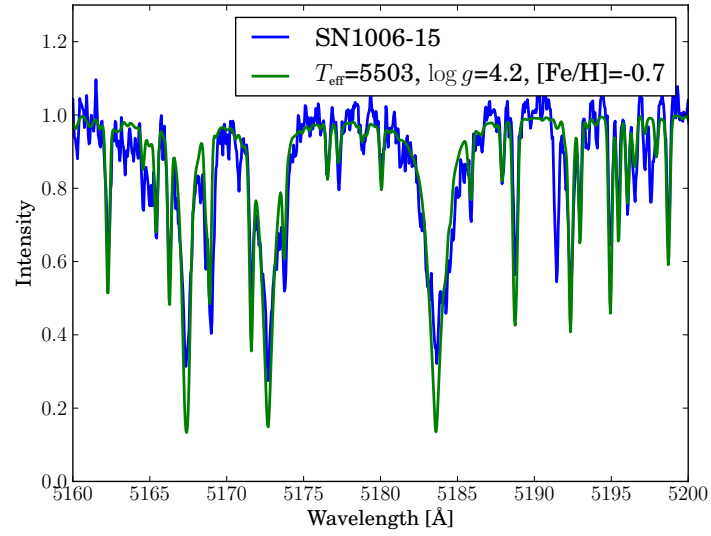
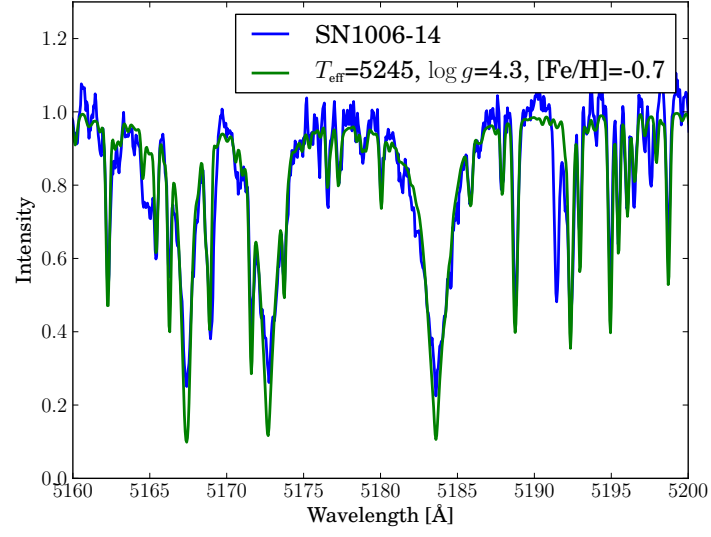
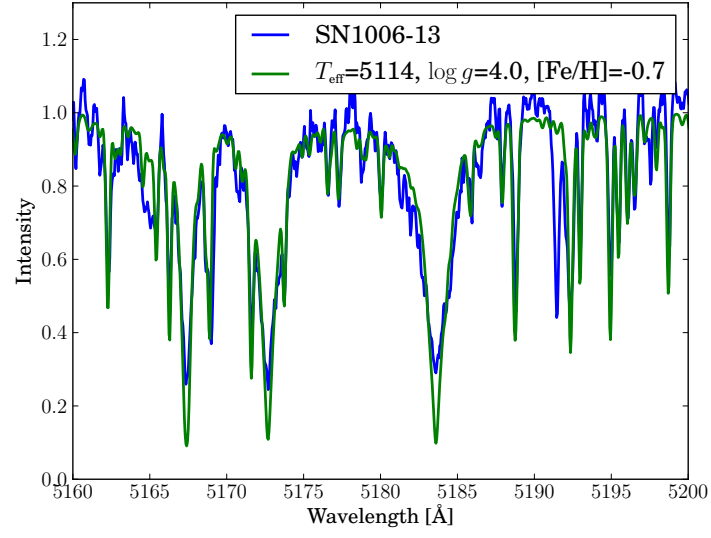


Figure 1.7 Fit of SN1006 candidate spectra

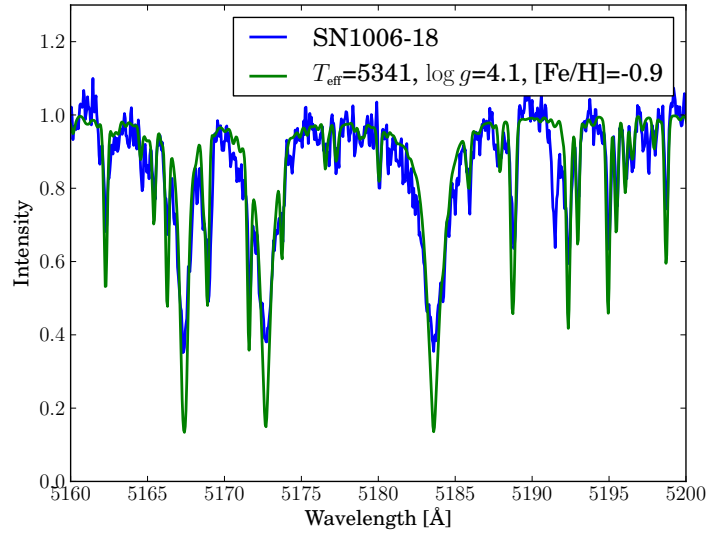
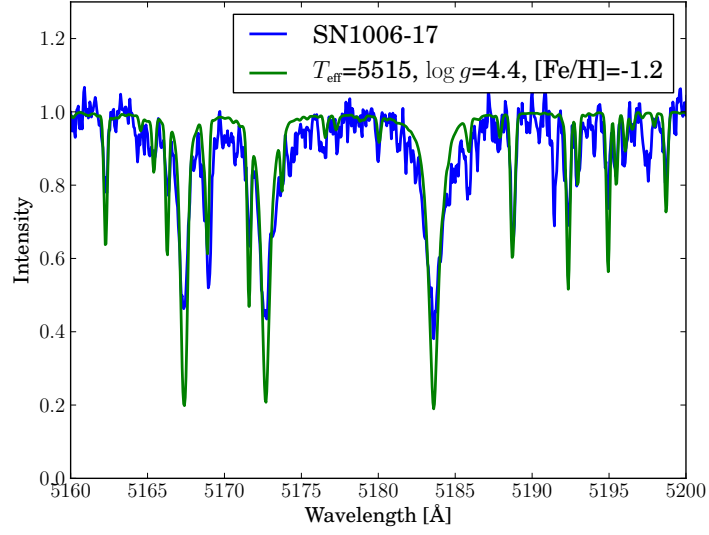
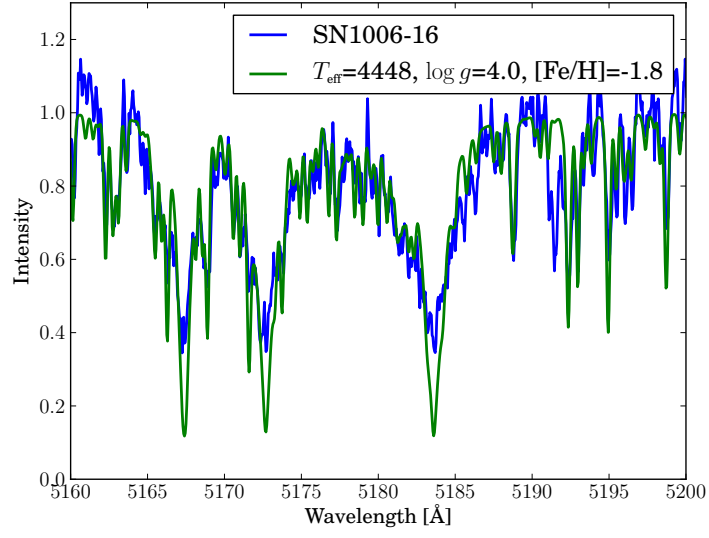


Figure 1.7 Fit of SN1006 candidate spectra

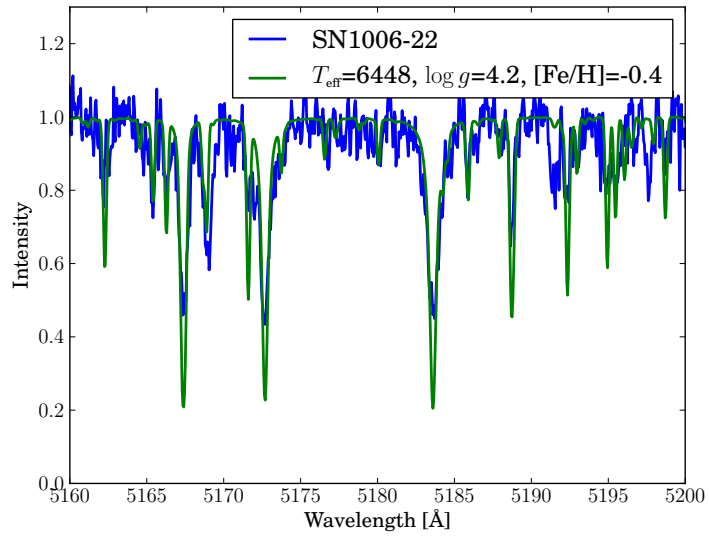
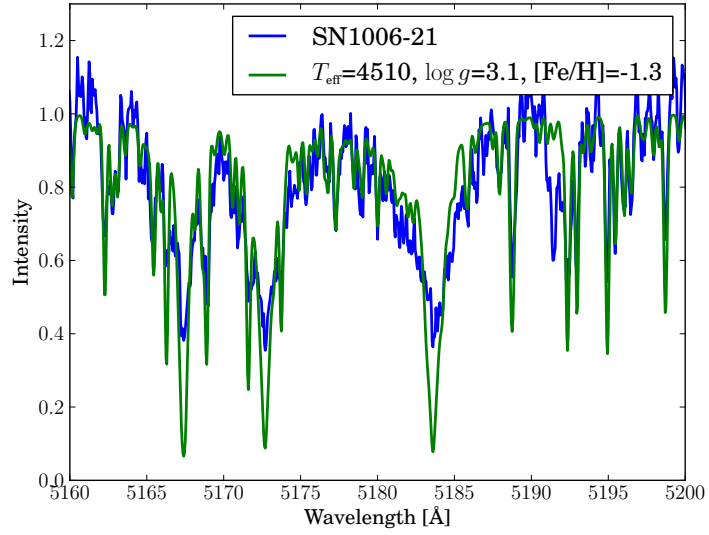
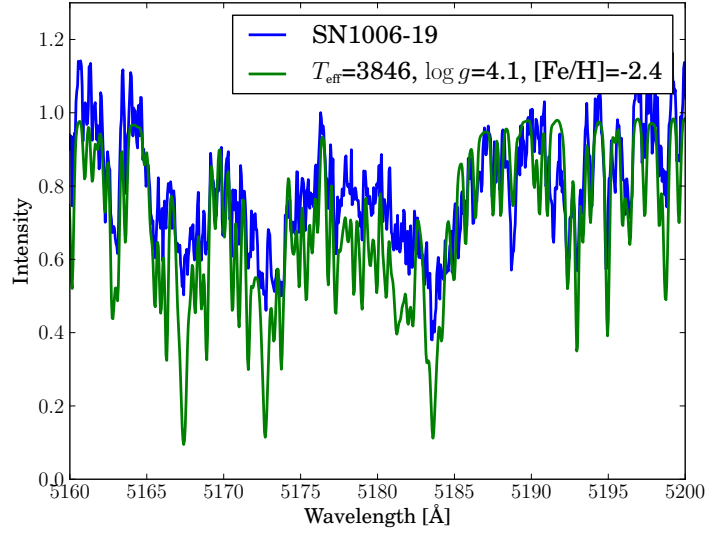


Figure 1.7 Fit of SN1006 candidate spectra

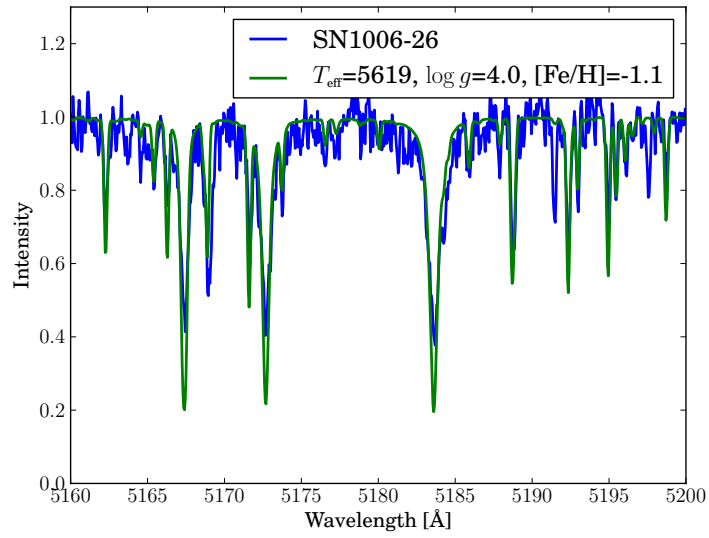
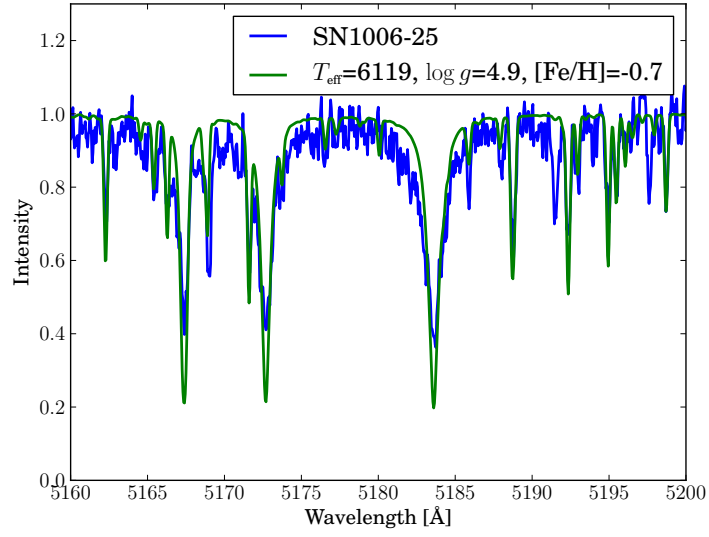
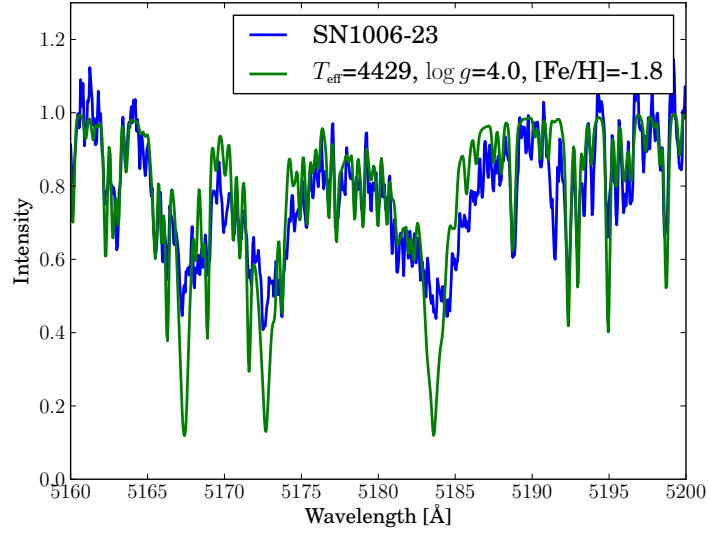


Figure 1.7 Fit of SN1006 candidate spectra

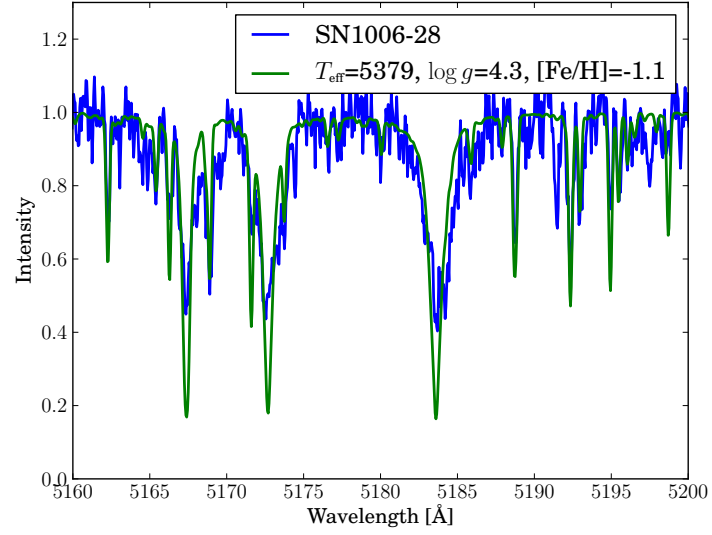
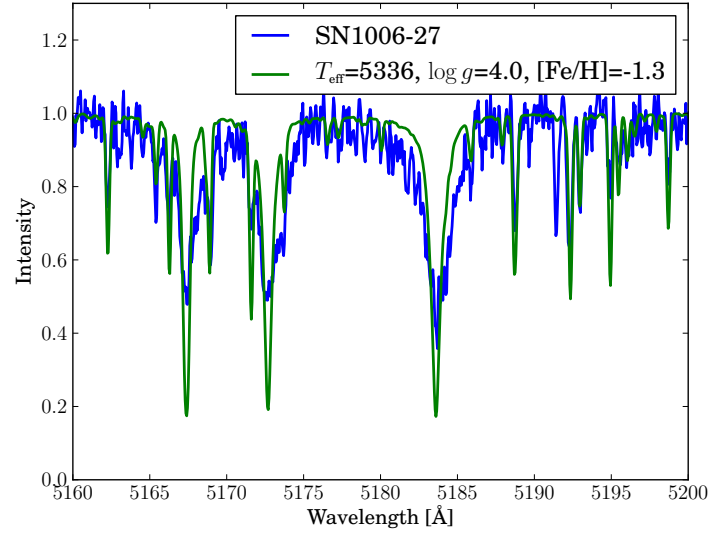


Figure 1.7 Fit of SN1006 candidate spectra

BIBLIOGRAPHY

- Barber, C. B., Dobkin, D. P., & Huhdanpaa, H. 1996, *ACM TRANSACTIONS ON MATHEMATICAL SOFTWARE*, 22, 469
- Casagrande, L., Ramírez, I., Meléndez, J., Bessell, M., & Asplund, M. 2010, *A&A*, 512, A54+ ([ADS entry](#))
- Castelli, F., & Kurucz, R. L. 2003, in *IAU Symposium*, Vol. 210, *Modelling of Stellar Atmospheres*, ed. N. Piskunov, W. W. Weiss, & D. F. Gray, 20P+ ([ADS entry](#))
- Goldstein, B. R., & Peng Yoke, H. 1965, *AJ*, 70, 748 ([ADS entry](#))
- Gray, D. F. 1977, *ApJ*, 211, 198 ([ADS entry](#))
- Gustafsson, B., Edvardsson, B., Eriksson, K., Jørgensen, U. G., Nordlund, Å., & Plez, B. 2008, *A&A*, 486, 951 ([ADS entry](#))
- Hamilton, A. J. S., Fesen, R. A., Wu, C.-C., Crenshaw, D. M., & Sarazin, C. L. 1997, *ApJ*, 481, 838 ([ADS entry](#))
- Han, Z. 2008, *ApJ*, 677, L109 ([ADS entry](#))
- Hinkle, K., Wallace, L., Valenti, J., & Harmer, D. 2000, *Visible and Near Infrared Atlas of the Arcturus Spectrum 3727-9300 Å*, ed. Hinkle, K., Wallace, L., Valenti, J., & Harmer, D. ([ADS entry](#))
- Kupka, F. G., Ryabchikova, T. A., Piskunov, N. E., Stempels, H. C., & Weiss, W. W. 2000, *Baltic Astronomy*, 9, 590 ([ADS entry](#))
- Kurucz, R., & Bell, B. 1995, *Atomic Line Data* (R.L. Kurucz and B. Bell) Kurucz CD-ROM No. 23. Cambridge, Mass.: Smithsonian Astrophysical Observatory, 1995., 23 ([ADS entry](#))
- Kurucz, R. L., Furenlid, I., Brault, J., & Testerman, L. 1984, *Solar flux atlas from 296 to 1300 nm*, ed. Kurucz, R. L., Furenlid, I., Brault, J., & Testerman, L. ([ADS entry](#))
- Maeda, K., Taubenberger, S., Sollerman, J., Mazzali, P. A., Leloudas, G., Nomoto, K., & Motohara, K. 2010, *ApJ*, 708, 1703 ([ADS entry](#))

- Marietta, E., Burrows, A., & Fryxell, B. 2000, *ApJS*, 128, 615 ([ADS entry](#))
- Pakmor, R., Röpke, F. K., Weiss, A., & Hillebrandt, W. 2008, *A&A*, 489, 943 ([ADS entry](#))
- Robin, A. C., Reylé, C., Derrière, S., & Picaud, S. 2003, *A&A*, 409, 523 ([ADS entry](#))
- Schweizer, F., & Middleditch, J. 1980, *ApJ*, 241, 1039 ([ADS entry](#))
- Skrutskie, M. F., et al. 2006, *ApJ*, 131, 1163 ([ADS entry](#))
- Snedden, C. 1973, *ApJ*, 184, 839 ([ADS entry](#))
- Tonry, J., & Davis, M. 1979, *AJ*, 84, 1511 ([ADS entry](#))
- van Dokkum, P. G. 2001, *PASP*, 113, 1420 ([ADS entry](#))
- Winkler, P. F., Gupta, G., & Long, K. S. 2003, *ApJ*, 585, 324 ([ADS entry](#))
- Winkler, P. F., Long, K. S., Hamilton, A. J. S., & Fesen, R. A. 2005, *ApJ*, 624, 189 ([ADS entry](#))
- Wu, C.-C., Crenshaw, D. M., Fesen, R. A., Hamilton, A. J. S., & Sarazin, C. L. 1993, *ApJ*, 416, 247 ([ADS entry](#))
- Wu, C.-C., Leventhal, M., Sarazin, C. L., & Gull, T. R. 1983, *ApJ*, 269, L5 ([ADS entry](#))